JACS Au
AN OPEN ACCESS JOURNAL OF THE AMERICAN CHEMICAL SOCIETY

pubs.acs.org/jacsau
Article

Enhanced Standard Operating Procedures for ^{31}P NMR-Based Metabolomics in Tissue Extracts

Sara Martin-Ramos, Jon Bilbao, Tammo Diercks, José M. Mato, Ganeko Bernardo-Seisdedos,* and Oscar Millet*

Cite This: JACS Au 2025, 5, 2285−2293
Read Online

ACCESS | Metrics & More | Article Recommendations | Supporting Information

ABSTRACT: Phosphorylated metabolites, here referred to as phosphometabolites, are sufficiently abundant and widely distributed to provide a condensed representation of metabolism that can be readily accessed through NMR spectroscopy. This study addresses the challenge of precisely quantifying phosphometabolites via quantitative ^{31}P NMR from tissue extracts. We optimized standard operating procedures for enhanced spectral resolution, signal intensity, and accuracy. By amply evaluating solvent and buffer conditions, reference compounds, and paramagnetic relaxation enhancers, we identified optimal conditions for metabolite analysis, including the use of trimethylphosphine oxide for accurate signal referencing due to its short T1 relaxation time and minimal offset and glycine buffer (in D_2O) at pD 9.5, where virtually invariant ^{31}P signal frequencies and sample osmolarities are observed, along with maximal NMR detection sensitivity and temperature stability of the pH. These methodological advancements significantly improve the reliability and reproducibility of phosphometabolite characterization, allowing the assignment of up to 60 independent signals in the one-dimensional (1D) ^{31}P spectrum (of a total of 94 peaks), that resulted in the proper quantification of 44 phosphometabolites from different tissular samples.

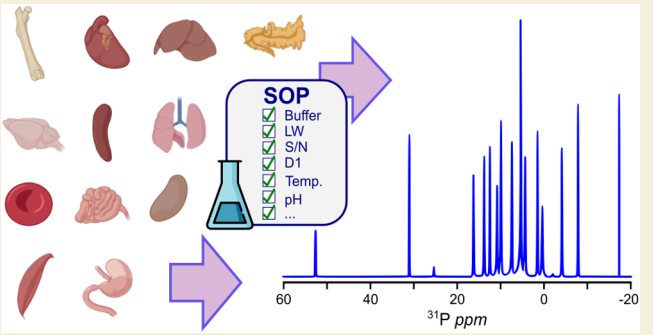

KEYWORDS: *^{31}P NMR, metabolites, glycine buffer, phosphorylated metabolites, tissue analysis, gadoteridol, SOP*

INTRODUCTION

Metabolomics, i.e., the comprehensive analysis of small molecules in biological systems, has emerged as a powerful tool to study diverse physiological and pathological processes.[1−4] A general complication, however, is the enormous amount of data generated by unselective approaches that target the entirety of metabolites, many of which may be of limited diagnostic value but greatly increase complexity. Selective techniques focusing on a subset of metabolites yield more manageable data that may much better disclose the relevant information. One important subset is the phosphorylated metabolites or phosphometabolites, which report on the energetic status and membrane constitution of cells as well as on diverse signaling pathways.[5−7] These highly informative phosphometabolites can be readily selected by ^{31}P NMR spectroscopy with direct quantification, large spectral dispersion, maximal spectral simplicity, and acceptable sensitivity. In practice, however, such studies are substantially complicated by the ^{31}P NMR signals' strong shifting with sample pH, osmolarity, and temperature, broadening from interaction with ubiquitous metal cations, overlap with chemically similar phosphometabolites, and recovery with unequal T_1 relaxation times compromising their quantifiability.[8−10] Thus, extreme caution must be applied to choose and control optimal sample conditions for phosphometabolite profiling studies by ^{31}P NMR.

Previous ^{31}P NMR studies have focused on enhancing spectral resolution and developing specific metabolite detection methods[11−13] and significant efforts were made to optimize experimental conditions for better detection of phosphometabolites and phospholipids.[13] Yet, these advances have often been limited to narrow applications without addressing the general challenges of quantitative ^{31}P NMR analysis in metabolomics.[14] This fragmentation in methodology causes increased variability and reduced reproducibility that limit the technique's utility for cross-sectional and longitudinal studies.[5,14]

We here expanded the available toolbox of ^{31}P NMR techniques,[13−15] to develop a set of standardized operating procedures (SOPs) applied to tissue samples and that enhance the accuracy, reliability, and reproducibility of phosphometa-

Received: March 3, 2025
Revised: April 3, 2025
Accepted: April 7, 2025
Published: April 13, 2025

bolite quantification, to ultimately leverage the inherent advantages of ^{31}P NMR for metabolic profiling. By systematically addressing factors such as solvent selection, buffer pH, temperature control, osmolarity correction, paramagnetic relaxation enhancer,[16] the use of appropriate reference compounds, and the optimization of two-dimensional (2D) ^{1}H−^{31}P correlational experiments for phosphometabolite recognition and signal assignment,[17] we found a set of experimental conditions that minimize chemical shift variability, facilitating the accurate identification and quantification of a wider range of phosphometabolites. The implementation of SOPs ensured consistent results across different tissue samples and studies, enhancing the reliability of metabolic profiling. Finally, our protocol addresses the critical need for accurate chemical shift referencing, providing a solid foundation for quantitative analysis.

MATERIALS AND METHODS

Chemicals

All chemicals and solvents used in this study were of analytical grade, and they are reported in Table S1.

Animal Models

Liver, kidney, spleen, muscle, intestine, brain, bone, lung, heart, stomach, pancreas, and blood extracts were obtained from male C57BL/6J mice raised for 8 months under standard dietary conditions. This specific mouse strain and age group was selected for their relevance in metabolic research and established use in previous liver metabolism studies.[17] Animal handling and experimental procedures strictly followed the guidelines of the institutional animal care and use committee (IACUC), which also gave approval prior to starting this study. At the conclusion of the rearing period, tissues were rapidly excised, flash-frozen in liquid nitrogen, and stored at −80 °C until their use for NMR analysis to preserve the biochemical sample integrity for accurate metabolomic profiling.

Metabolic Extraction

For the extraction of metabolites from different tissues we employed a dual-phase extraction protocol to isolate both hydrophilic and lipophilic metabolites efficiently, as described before.[18] Approximately 100 mg of liver tissue (unless otherwise indicated) were lysed in 774 μL of an ice-cold $CHCl_3/CH_3OH$ mixture (38.8/61.2 v/v%), supplemented with 254 nmol of DSS for internal standardization. For tissue lysis in a Precellys tissue homogenizer, we used specific ceramic zirconium oxide beads of variable diameter depending on the tissue: 1.4 mm for liver, brain, kidney, and lung; 2.8 mm for bone, heart, intestine, pancreas, stomach, and muscle; mix of 2.8 and 5.0 mm for spleen. We applied two 30 s cycles at 6000 rpm to ensure thorough disruption of cellular structures. Following lysis, 554 μL of $CDCl_3/H_2O$ mixture (45.8/54.2 v/v%) were added to the homogenate to facilitate phase separation. The mixture was then incubated on dry ice for 15 min to enhance metabolite precipitation, followed by centrifugation at 14,000 rpm for 15 min at 4 °C to fully separate the biphasic components. Aqueous and organic phases were collected and transferred to new tubes. To concentrate the extracted metabolites and remove solvents, the separated phases were dried in a vacuum concentrator at room temperature for approximately 3 h. This step was critical to remove all solvents and to obtain dry extracts suitable for subsequent ^{31}P NMR spectroscopic analysis.

NMR Sample Preparation

For the hydrophilic extracts of liver tissue (E1), the finally established composition was: (i) solvent: D_2O; (ii) buffer: Glycine pD 9.5 (50 mM); (iii) chelator: EDTA (2 mM); (iv) PRE: Gdter (0.5 mM); (v) *standard*: TMP^+ (1 mM) and $OPMe_3$ (1 mM) were used for ^{31}P chemical shift referencing and signal quantification. For individual component testing, the concentrations of the chelator (EDTA) and PRE agent (Gdter or Gdbut) were varied independently. Similarly, the following buffers, sorted by increasing pH, were tested in D_2O: 50 mM $H_2AsO_4^-$ pD 2.2 (50 mM), acetate pD 4.5 (50 mM), 50 mM $HAsO_4^{2-}$ pD 7.0 (50 mM), Tris-d_{11} pD 7.0 (100 mM), glycine pD 9.5 (50 mM), CO_3^{2-}/HCO_3^- pD 10 (50 mM), and AsO_4^{3-} pD 11.5 (50 mM).

For the hydrophobic extracts of liver tissue (E2), the following pure organic solvents, sorted by increasing dipole moment were tested in perdeuterated form to allow for magnetic field locking: toluene-d_8, $CDCl_3$, n-hexanol, THF-d_8, CD_3OD, acetone, DMSO-d_6 or undeuterated and combined with a 5% of $CDCl_3$: n-hexanol, acetone. Similarly, mixtures of methanol and chloroform were tested by adding the former to a sample prepared in pure $CDCl_3$ up to volume ratios of 1:10, 2:10, 4:10, 6:10, and 10:10. Finally, the CUBO "solvent system"[15] was also included in the analysis.

Osmolality Determination

The osmolality of 114 processed liver samples was measured using a Gonotec Osmomat Freezing Point Osmometer Model 3000. Two calibration standards (300 mOsmol/kg NaCl/H_2O and 850 mOsmol/kg NaCl/H_2O, Gonotec) were employed for osmometer calibration. A calibration curve was then obtained by measuring different concentrations of NaCl in D_2O (0, 50, 100, 150, 200, 250, and 300 mM).

NMR Spectroscopy

All NMR experiments were performed on a Bruker Avance NEO 600 MHz spectrometer equipped with a dual ^{1}H, BB broadband observe (BBO) probehead (with *z*-gradient coil and automatic tuning and matching accessory) for maximal ^{31}P detection sensitivity and with an automatic sample changer (SampleCase). Default temperatures were 288 K for hydrophilic liver extract samples and 310 K for lipophilic liver extract samples. The following NMR experiments were recorded: (i) one-dimensional (1D) ^{1}H{^{31}P} with water presaturation and ^{31}P decoupling (GARP4 with B_{RF} = 3.333 Hz; modified BRUKER pulse program *noesygppr1d*); (ii) 1D ^{31}P{^{1}H} with ^{1}H decoupling (DIPSI2 with B_{RF} = 1.800 Hz; modified BRUKER pulse program *zgig*); (iii) 2D ^{1}H,^{31}P-HSQMBC-TOCSY implementing CPMG-INEPT (70 ms, B_{CPMG} = 925 Hz) and subsequent ^{1}H,^{1}H MOCCA-z-TOCSY (100 ms, B_{MOCCA} = 3.500 Hz); (iv) pseudo-2D ^{31}P{^{1}H} inversion recovery (modified BRUKER pulse program *invrec*). For a selected group of samples and to assist in the assignment, the spectral data set also included a 2D ^{1}H,^{1}H-TOCSY (100 ms, 8 scans, 128 dummy scans, 1.5 s interscan delay). In the evaluation of the temperature effect on the PRE agent, the acquisition protocol was designed for precision, entailing 8 scans, 32 dummy scans, and a 4 s interscan delay for 1D spectra, complemented by *invrec* experiments conducted with 512 scans.

RESULTS AND DISCUSSION

Overall Strategy

To optimize the experimental conditions, we have considered the following quality factors: (1) *repeatability* of the overall method; (2) signal dispersion, defined as the number of isolated signals (i.e., nonoverlapping) that can be univocally quantified; (3) an adequate signal-to-noise ratio (S/N) and line width (T_2) to ensure their quantification; and (4) *reproducibility*, which refers to the chemical shift's insensitivity to buffer conditions. The latter is particularly crucial, since biological tissues may present a wide range of conditions, such as varying osmolarity.

Tissue Extraction

Tissular extracts were resuspended in $CHCl_3/CH_3OH$ (38.8/61.2 v/v%), adding DSS for internal standardization, and subsequently homogenized (see the Materials and Methods Section). The homogenate was then diluted in $CDCl_3/H_2O$ (45.8/54.2 v/v%) to facilitate phase separation. Biphasic extraction allowed separation of the hydrophilic (E1) and

https://doi.org/10.1021/jacsau.5c00234
JACS Au 2025, 5, 2285−2293

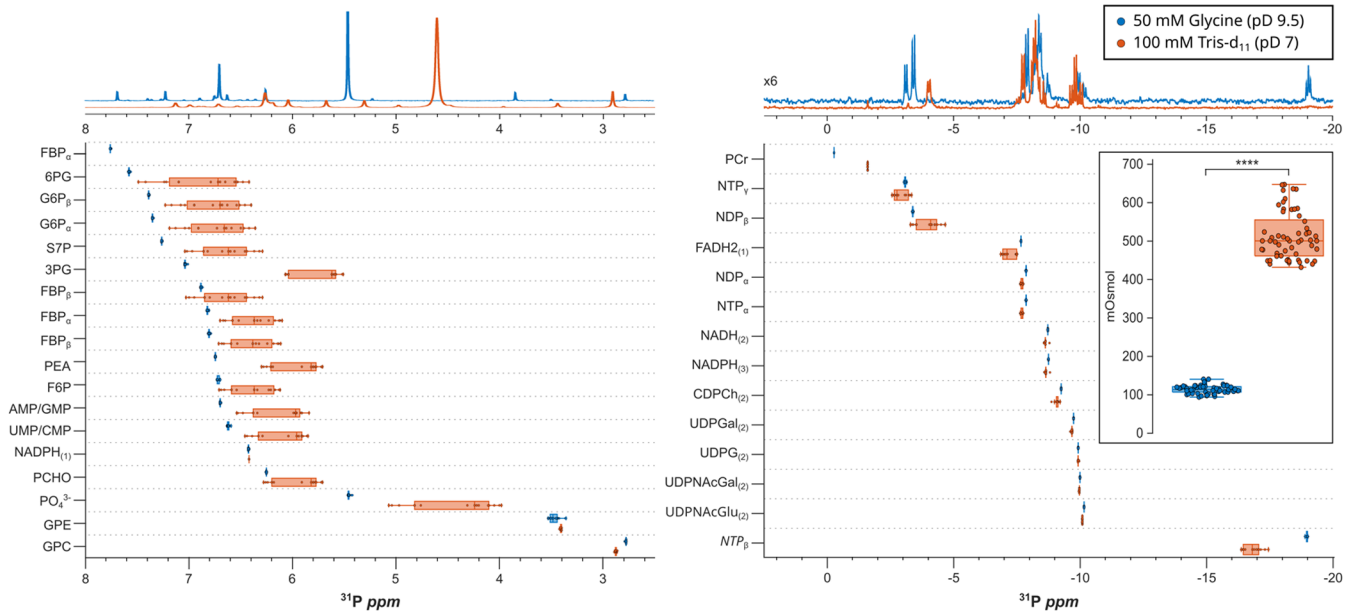

Figure 1. Comparative analysis of the phosphometabolite chemical shifts and sample osmolality in different buffers (reproducibility). Box plots depict the ^{31}P chemical shift distributions for various phosphometabolites in 50 mM glycine (pD 9.5, n = 57, blue) and 100 mM tris-d_{11} (pD 7.0, n = 15, orange), underlining the larger chemical shift heterogeneity observed in the tris-d_{11} buffer. Inset: osmolality distribution from 114 liver samples (57 per buffer group); Tris-d_{11} buffer not only shows a broader range of osmolality values but also higher median values, confirming the buffer's influence on the overall sample conductivity.

hydrophobic (E2) extracts, which are treated independently, maximizing the number of phosphometabolites under consideration. The hydrophilic phase contains phosphometabolites that are generally small, polar molecules such as phosphorylated monosaccharides, amino acids, nucleotides, etc., while the hydrophobic phase phosphometabolites cover a wide range of molecular sizes, from small to very large (as in waxes), and amphiphilic properties, from moderate to vanishing residual local polarity.

Phosphometabolites are very sensitive to the tissue extraction protocol, and some protocols may result in incomplete extraction. Ischemia and residual enzyme activity may result in the *biochemical* alteration of the metabolite composition, especially in energy-related phosphometabolites. Therefore, excised tissues were immediately frozen in liquid nitrogen. Moreover, the extraction method requires the use of a cell disruptor, which may induce the *chemical* hydrolysis of some phosphometabolites such as ATP or NADPH.[19] To test for repeatability and accuracy, a single liver sample was divided into ten samples that were processed and analyzed independently to quantify the phosphometabolites (Table S2). The repeatability of the overall extraction methodology is high (with about 8% of the overall variability and around 12% variability in the more labile metabolites, Figure S1). Attempts to use milder extraction methods resulted in incomplete metabolite extraction, showing a nonrepresentative phosphometabolite composition of the tissue.

Solvent and Buffer Selection

For the E1 extract, we first assessed the use of buffers in H_2O versus D_2O. Using D_2O has the advantage that we can also complement the metabolism characterization, based solely on phosphometabolites, with a few very relevant metabolites that can directly and easily be quantified from the ^{1}H NMR spectrum (i.e., lactate, glucose, choline, and total cholesterol). In our comparative analysis of solvent effects, utilizing a plethora of buffers in D_2O versus H_2O, we revealed nuanced differences in signal intensities for key phosphometabolites: D_2O exhibited a decrease in signal intensity for GPE when compared to H_2O, while FBP showed the opposite trend (Table S2). That said, most of the analyzed metabolites showed a solvent dependence intensity lower than 10%, and line width measurements of phosphometabolites in D_2O and H_2O indicated negligible variance in signal quality across the two solvents (Figure S2), suggesting that both solvents are suitable for ^{31}P NMR analysis based purely on line width criteria. Given these considerations, D_2O was selected over H_2O as the preferred solvent for our optimized ^{31}P NMR methodology.

We then assessed several buffers including $H_2AsO_4^-$ at (uncorrected) pD 2.2, acetate at pD 4.5, $HAsO_4^{2-}$ and tris-d_{11} at pD 7, glycine at pD 9.5, CO_3^{2-}/HCO_3^- pD 10, and AsO_4^{3-} at pD 11.5, expanding the previously studied range of buffers (acetate and bicarbonate).[13,29] Phosphometabolite signal intensity and dispersion significantly improved at extreme pD (pH) conditions, and we found the best results under a moderately basic environment (Figure S3). Notably, specific ^{31}P signals critical for phosphometabolite profiling studies, such as doublets in the phosphodiester region around −3.5 ppm and triplets from P-β in nucleoside triphosphates (NTP) around −19 ppm, were exclusively observed in settings with an uncorrected pD greater than 7.

Among the tested basic buffers, we found that glycine best performs. Glycine buffer increases the capacity of chelating agents to complex with cations because of the high pH levels that enhance deprotonation[20,21] and, to a lesser extent, to coordinate monovalent cations through the amine group.[22] These synergistic effects result in a reduced concentration of circulating free cations. To test this hypothesis, we determined the osmolality for a set of 114 liver tissue extracts processed in tris-d_{11} buffer (pD 7.0, n = 57), as previously employed,[18] or in

https://doi.org/10.1021/jacsau.5c00234
JACS Au 2025, 5, 2285−2293

glycine buffer (pD 9.5, $n = 57$) (Figure 1, inset). Glycine buffer at pD 9.5 has a low intrinsic conductivity and, consequently, showed a much lower value of average osmolality as compared with tris-d_{11} buffer. Remarkably, it also showed a much less intersample osmolality variability, suggesting that it should also reduce the chemical shift dispersion within samples. Indeed, the ^{31}P NMR spectra in glycine buffer showed negligible dispersion in the chemical shift values of the assigned metabolites (Figure 1, blue bars) as compared to the chemical shift variation observed in tris-d_{11} buffer (Figure 1, orange bars). Finally, glycine buffer has minimal B_{RF} losses,[20,22] as evidenced by the shortest ^{1}H pulses, and this buffer largely preserves the metabolite mixture for at least 120 h at room temperature (Figure S4). Altogether, 50 mM glycine buffer at pD of 9.5 was identified as an optimal medium for the hydrophilic phosphometabolite profiling studies.

In hydrophobic extracts, it is customary to use the same extraction ternary system ($CHCl_3$:MeOH:H_2O) as a solvent for spectroscopical characterization.[15,23] Yet, we decided to resuspend the E2 extract in pure aprotic solvents to avoid phase separation.[12] Explored solvents included toluene-d_8, THF-d_8, $CDCl_3$, 1-hexanol, CD_3OD, acetone, DMSO-d_6 and the CUBO 'solvent system'.[12,15] Our findings revealed a direct correlation between the solvent's dipolar moment (μ) and the ^{31}P signal dispersion and intensity (Figure S5). Particularly, solvents with low μ, such as toluene-d_8, $CDCl_3$, and THF-d_8, affected the spectral quality adversely, suggesting a tendency to form inverse micelles. Acetone exhibited good peak dispersity but caused significant line broadening, which may indicate improper dissolution of lipid mixtures. Among the solvents evaluated, DMSO-d_6 stood out due to its high dipolar moment (3.96 D) and its ability to significantly improve both the signal intensity and dispersion of ^{31}P NMR spectra of E2 liver extracts, including the signals of TPPO and various phospholipids (Figure S5). Interestingly, the CUBO system also provides a well-resolved spectrum, but it was discarded due to the risk for gradual hydrolysis of carboester bonds (i.e., converting glycerolipids into glycerolysolipids).[24]

Chelating Agents

The presence of divalent cations such as Mg^{2+} and Ca^{2+} in E1 liver extracts can significantly influence ^{31}P NMR signals due to their interaction with phosphate groups.[25] These interactions can lead to signal shifts and broadenings, which may complicate the analysis and quantification of the phosphometabolites. One solution is to saturate with divalent cations[13] but we opted for a chelating agent,[26] since divalent ions catalyze phosphoester hydrolysis and because of the synergistic mechanism observed with the glycine buffer (vide supra). The investigation focused on the impact of different EDTA or CDTA concentrations (0, 1, and 2 mM) on the signal intensities across four characteristic regions of the ^{31}P spectrum: monophosphates, diphosphodiesters, orthodiphosphodiesters, and P_β in NTPs. In line with previous studies,[29] our findings with EDTA (Figure S6) revealed that 1 mM concentration significantly enhanced ^{31}P signal intensities, particularly in diphosphodiesters, orthophosphodiesters, and P_β in NTP regions. Increasing the EDTA concentration up to 2 mM resulted in slight signal shifts, suggesting additional cation sequestration; therefore, this concentration was selected for our SOPs. CDTA was discarded due to its lower chelator capacity compared to that of EDTA (data not shown).

Reference Compounds for Quantification

Reference compounds are required for quantitative analysis of metabolites.[27] A paramount feature of an effective reference compound is a short $T_1(^{31}P)$ relaxation time for rapid signal recovery. For the E1 extract, our investigation focused on TMP^+, $OPMe_3$, and $OPEt_3$ due to their potential for providing sharp and distinct ^{31}P signals, which are crucial for accurate frequency referencing (Table S3).

TMP^+ exhibits a ^{31}P signal at 25.86 ppm, with its ^{1}H signal at 1.790 ppm, showcasing its clear separation from metabolite signals. $OPMe_3$, however, offers a slightly different ^{1}H signal at 1.586 ppm, with no direct ^{31}P signal comparison provided in the excerpt ($\delta_{31P} = 56.10$ ppm), but its selection was ultimately justified by its superior properties for quantitative analysis. $OPEt_3$ produces two ^{1}H signals (1.82 ppm (q) and 1.105 ppm (t)), potentially complicating the analysis due to overlap with tissue metabolite signals. The decision to select $OPMe_3$ over TMP^+ and $OPEt_3$ was substantiated by its minimal ^{31}P offset and short T_1 relaxation times (5.4 s), facilitating rapid signal recovery, which is essential for quantitative referencing. However, TMP^+ or the previously reported methylene diphosphonate[28] are also viable alternate reference compounds, due to their low pH dependence.

When considering the E2 extracts, we identified triphenylphosphine oxide (TPPO) as an adequate choice. TPPO exhibits a sharp singlet signal at 28.59 ppm, significantly distanced from the signals of most metabolites, which is critical for clear, unambiguous quantification. In addition, TPPO's $T_1(^{31}P)$ relaxation time of 1.3 s (at 310 K, vide infra) proved to be ideal, facilitating efficient and accurate quantitative referencing across the analyses.

PRE Additives and Temperature Optimization

The addition of PRE agents enhances T_1 relaxation, and its use in quantitative metabolomics has been suggested.[29] We here explored the use of Gdter and Gdbut as PRE agents. Key to our analysis was the balance between accelerating T_1 relaxation times for enhanced sensitivity and minimizing the effect on T_2 relaxation times to prevent signal broadening. First, experimental evaluations were conducted at varying concentrations of Gdter and Gdbut (0, 0.5, 1.0, and 1.5 mM) at 298 K in 5 mM standard mixtures. The results show that Gdbut effectively reduces T_1 relaxation times for polar phosphometabolites such as AMP but leads to increased ^{31}P signal half-width (Figure S7). Conversely, Gdter presents a balanced profile, significantly accelerating T_1 relaxation without adversely impacting T_2 relaxation, thus maintaining the integrity of ^{31}P signals. A systematic evaluation of the different conditions (Tables S4, S5, Figures S8 and S9) yielded 0.5 mM Gdter as the most effective concentration, providing an optimal balance by optimizing T_1 relaxation times without compromising the signal quality.

We then evaluated the dependence of temperature on the PRE effect. To that end, E1 liver extracts were prepared in a 50 mM glycine buffer at uncorrected pD 9.5, supplemented with 1 mM $OPMe_3$, 1 mM TMP^+, and 2 mM EDTA. We examined the impact of varying Gdter concentrations (0, 0.5, and 1 mM) across a temperature range (278−308 K), (Figures S8 and S9). Consistent with previous studies,[13] data analysis revealed a preference for lower temperatures in the absence of Gdter, generally leading to reduced T_1 relaxation times and signal half-width, thus enhancing signal intensities for key phosphometabolites, including methylphosphate (MPHO), UMP, and

https://doi.org/10.1021/jacsau.5c00234
JACS Au 2025, 5, 2285−2293

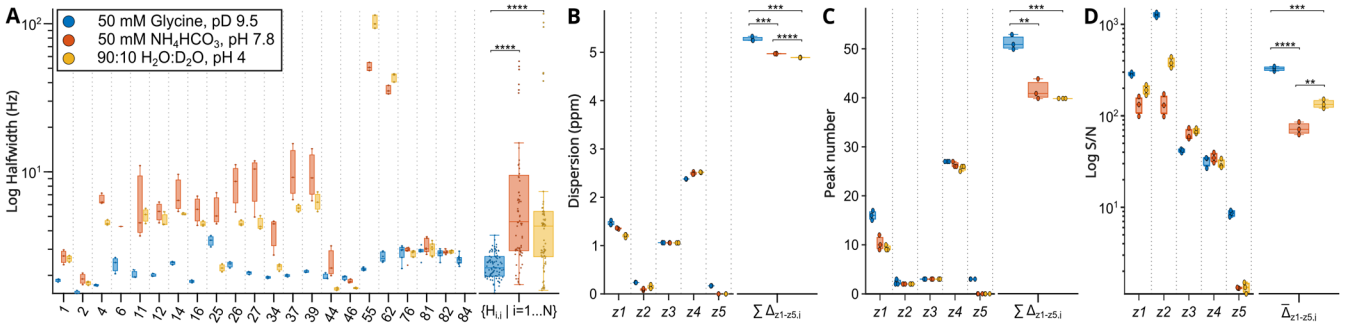

Figure 2. Effect of buffer composition on phosphometabolite quantification in a mouse liver extract. The same mouse liver extract was resuspended in three different buffers: 50 mM glycine, 0.5 mM Gdter, and 2 mM EDTA (pD 9.5, blue); 50 mM NH_4HCO_3 (pH 7.8, red);[29] and water/HCl (pH 4, black and yellow).[11] The impact of these buffers was evaluated based on several parameters, including half-width determination for 21 independent peaks (A), peak dispersion (B), the number of independent peaks that require no deconvolution with a signal-to-noise ratio (S/N) > 4 (C), and S/N ratio analysis of triplicates for $z1$ to $z5$, corresponding to the ^{31}P chemical shift ranges of 8−6 ppm ($z1$), 5.5−4 ppm ($z2$), 4−2.5 ppm ($z3$), −7.6 to −10.5 ppm ($z4$), and −18.5 to −19.5 ppm ($z5$), respectively (D). For each parameter, the appropriate statistical comparison is shown in the right part of the figure. If the change is statistically significant, it is indicated by asterisk symbols (*: adjusted p-value less than 0.05; **: p-value <0.01; ***: p-value <0.001; ****: p-value <0.0001).

CMP. Notably, at 278 K, these metabolites exhibited the most pronounced intensity levels, highlighting the benefits of lower temperatures for superior signal clarity and quantification accuracy. MPHO, known for its prolonged T_1 relaxation time, showed a marked reduction in T_1 across all temperatures with 0.5 mM Gdter, reaching acceptably short T_1 times (<1.5 s) at 1 mM Gdter and lower temperatures. Furthermore, the interplay between Gdter concentration and temperature demonstrated a decrease in the required amount of Gdter with decreasing temperature, due to the natural shortening of T_1 times in cooler conditions, confirming that 0.5 mM of Gdter at 288 K offers a balanced approach, reducing T_1 times without adversely affecting signal quality due to T_2 broadening.

Albeit its limited solubility, the impact of Gdter was also assessed for its influence on ^{31}P NMR signal quality in the E2 extract, resuspended in DMSO-d_6 at 298 K. The introduction of 0.05 mM, was scrutinized for its effect on signal integrity, focusing on the half-width (T_2) of ^{31}P NMR signals. The addition of little amounts of PRE agent already resulted in significant line broadening, and it was discarded.

The influence of temperature on the ^{31}P NMR spectral analysis of E2 extracts from mouse liver was also investigated in the absence of PREs, to optimize the detection and quantification of phospholipid metabolites. A range of temperatures (298, 303, 308, 313, 318, and 323 K), was considered to determine the optimal temperature that would enhance signal intensity and resolution, while balancing the relaxation times (T_1 and T_2) of the phospholipids, excluding triphenylphosphine oxide (TPPO). Our findings (Table S6 and Figure S10) reveal that the peak signal intensities for key phospholipids such as phosphatidylcholine (PC), phosphatidylethanolamine (PE), lysophosphatidylcholine (LPC), sphingomyelin (SM), and lysophosphatidylethanolamine (LPE) were significantly affected by the temperature, with the highest intensity for these phospholipid signals observed at 310 K.

Optimization of the Iterscan Delay (d_1)

Finally, our SOPs also included optimization of the delay time d_1, also known as the relaxation delay, which allows nuclear spins to fully relax before being pulsed again and is critical for accurate quantification in ^{31}P NMR analysis. Precise quantification requires an interscan delay $d_1 > 3{\cdot}T_{1,\max}(^{31}\mathrm{P})$ to achieve maximal signal-to-noise ratio ($S/N_{max} \approx 1/\sqrt{d_1}$ at $d_1 = 1.25{\cdot}T_1(^{31}\mathrm{P})$). For the E1 extract, with the optimized Gdter concentration at 0.5 mM and a temperature of 288 K, the necessary relaxation delay for over 95% recovery of the slowest relaxing species, such as MPHO and the reference compound for quantification ($OPMe_3$), was determined to be 7.0 s (Table S7). This was based on achieving an equilibrium between signal recovery and quantification accuracy considering the slowest relaxing species MPHO across a range of Gdter concentrations and temperatures.

Simulations were conducted to assess the final d_1 for quantitative analysis under standard conditions (600 MHz, 288 K, 0.5 mM Gdter, 2 mM EDTA, 50 mM glycine buffer pD 9.5) for both the slowest (MPHO) and fastest (UDPG) relaxing species revealed critical insights (Figure S11). With a minimal single-scan S/N of either 1.1 or 2 and a total experiment time of 6 h, the quantification error for the slowest relaxing species (MPHO) remained marginal and unchanged at d_1 = 7s, indicating no time wastage for these species. However, for the faster relaxing species with low S/N, significant time wastage occurred, necessitating a reduction in d_1 to 6 s to mitigate the increased quantification error.

The optimization of d_1 in the E2 extract was conducted in DMSO-d_6 at a temperature of 310 K, measuring the longitudinal relaxation times (T_1) of TPPO, LPC, and PC standards (Table S8). The longest relaxation time, belonging to TPPO, dictates the minimum d_1 required to ensure full relaxation and accurate quantification of all metabolites within the sample. Based on the above-mentioned principle for the relaxation time ($>3 \times T_{1,\max}$), and considering TPPO's T_1 of 1.3 s as $T_{1,\max}$, we found a minimal d_1 of 5 s. This duration ensures that all phosphometabolites, especially those with longer T_1 times, are fully relaxed before the next scan commences.

Performance of the Methodology

We compared the methodology presented here with other available methods for the NMR analysis of phosphorylated metabolites,[13,29] using equivalent samples from the same mouse liver and maintaining a fixed acquisition time of 6 h. It is important to emphasize that the published methods were not specifically optimized for tissue samples. The overlay of the spectra is shown in Figure S12, while Figure 2 reports on the analysis results, including the analysis for statistical significance.

https://doi.org/10.1021/jacsau.5c00234
JACS Au 2025, 5, 2285−2293

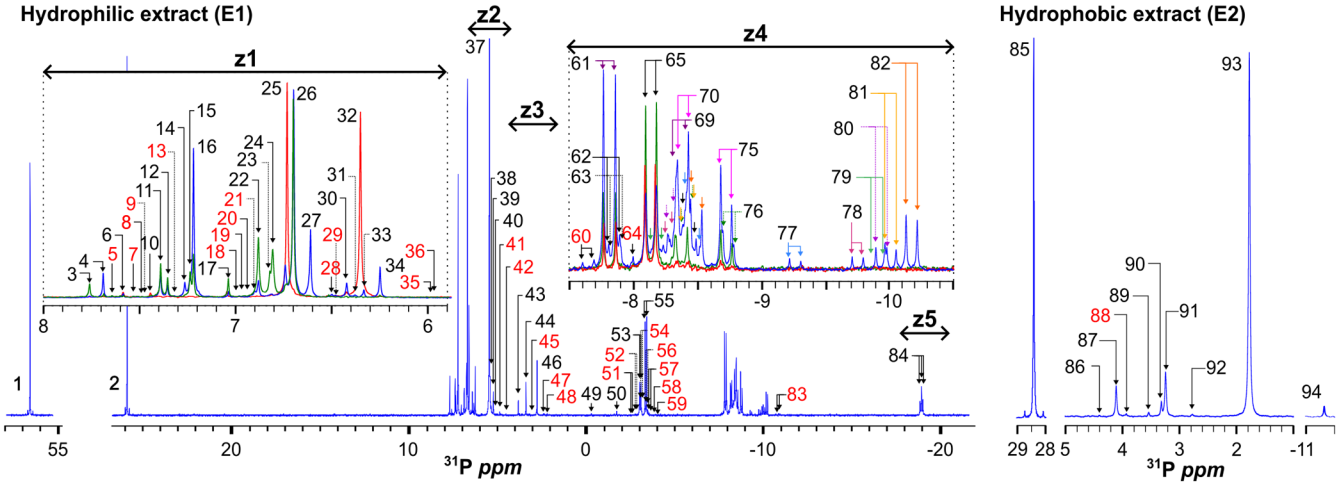

1 $OPMe_3$	15 M6P	29 unk10 p.	43 unk18 p.	57 unk26 p.	71 $CoA_{(3)}$*	85 TPPO
2 TMP^+	16 G3P	30 $NADPH_{(1)}$	44 GPE*	58 unk27 p.	72 $NADH_{(1)}$ / $UDPNAcGal_{(1)}$*	86 LPE
3 $FBP_{(\alpha)}$	17 3PG	31 unk11 p.	45 unk19 p.	59 unk28 p.	73 $CDPCh_{(1)}$*	87 PI
4 MPHO*	18 unk06 p.	32 2,3-$BPG_{(2)}$	46 GPC	60 unk29 p.	74 $UDPNAcGlu_{(1)}$*	88 unk33 p.
5 unk01 p.	19 unk07 p.	33 unk12 p.	47 unk20 p.	61 $FADH2_{(1)}$*	75 $NADPH_{(3)}$	89 SM
6 6PG*	20 unk08 p.	34 PCHO	48 PEP	62 $NDP_{(\alpha)}$	76 $NADH_{(2)}$	90 LPC
7 FMN	21 F1P*	35 unk13 p.	49 PCr	63 $CoA_{(2)}$* / unk30 p.	77 $CDPCh_{(2)}$*	91 PE / CL
8 unk02 p.	22 $CoA_{(1)}$* / $FBP_{(\beta)}$	36 unk14 p.	50 unk21 p.	64 unk31 p.	78 $UDPGal_{(2)}$*	92 $LPC_{(isomer)}$
9 unk03 p.	23 $FBP_{(\alpha)}$	37 PO_4^{3-}	51 unk22 p.	65 $NTP_{(\alpha)}$	79 $UDPGA_{(2)}$*	93 PC
10 unk04 p.	24 $FBP_{(\beta)}$	38 Gal1P*	52 unk23 p.	66 $UDPGA_{(1)}$*	80 $UDPG_{(2)}$	94 unk34 p.
11 $G6P_{(\alpha)}$	25 PEA* / F6P / 2,3-$BPG_{(1)}$	39 R1P*	53 $NTP_{(\gamma)}$	67 $UDPGal_{(1)}$	81 $UDPNAcGal_{(2)}$*	
12 $G6P_{(\beta)}$	26 AMP / GMP	40 unk15 p.	54 unk24 p.	68 $UDPG_{(1)}$	82 $UDPNAcGlu_{(2)}$*	
13 unk05 p.	27 UMP / CMP*	41 unk16 p.	55 $NDP_{(\beta)}$	69 $FADH2_{(2)}$*	83 unk32 p.	
14 S7P*	28 unk09 p.	42 unk17 p.	56 unk25 p.	70 $NADPH_{(2)}$	84 $NTP_{(\beta)}$	

Figure 3. ^{31}P NMR spectroscopy of representative mouse tissue extracts. A total of 94 peaks were unambiguously detected and 46 of them were assigned to different phosphometabolites. Metabolites that are first reported in this study are highlighted with a blue asterisk. In blue, the ^{31}P NMR spectrum of 300 mg of liver extract is shown. Red spectrum corresponds to blood whereas green spectrum corresponds to muscle. **E1** is analyzed in 50 mM glycine-d_2 at pD 9.5 (in D_2O), 0.5 mM Gdter, 2 mM EDTA, at 288 K, and an interscan delay of 6 s. **E2** is analyzed in DMSO-d_6 at 310 K with a d_1 of 5 s. Red numbers in the spectra represent metabolites with an S/N < 5 in a 100 mg sample. 81.8% of the unknown peaks (unk p.) are under an S/N < 5. Selected regions of the spectra ($z1$−$z5$), correspond to chemical shift ranges 8−6 ppm ($z1$), 5.5−4 ppm ($z2$), 4−2.5 ppm ($z3$), −7.6 to −10.5 ppm ($z4$), and −18.5 to −19.5 ppm ($z5$).

P-values for the different comparisons are shown in Table S9. For comparison purposes, the spectrum was divided into five regions: $z1$ to $z5$ corresponding to ^{31}P chemical shift ranges 8 to 6, 5.5 to 4, 4 to 2.5, −7.6 to −10.5, and −18.5 to −19.5 ppm, respectively (Figure 3). The glycine buffer exhibits a similar peak dispersion to other methods (Figure 2B) but produces sharper peaks (Figure 2A). As a result, a statistically significant larger number of isolated peaks can be integrated unequivocally without the need for deconvolution methods (Figure 2C). In terms of the S/N ratio, the glycine buffer performs better in general (Figure 2D), outperforming in regions $z1$, $z2$, and $z5$, while being less sensitive in region $z3$. In addition, the use of glycine buffer ensures optimal reproducibility (Figure 1), and the repeatability of the overall methodology is approximately 90% (Figure S1). Finally, the conditions optimized here for ^{31}P NMR also yield high-quality spectra suitable for ^{1}H NMR-based metabolomics studies (when using deuterated glycine, Figure S13).

NMR Assignment Strategy and Quantification of the Phosphometabolites

We have used our set of optimized conditions (i.e., 50 mM glycine-d_2 at pD 9.5 (in D_2O), 0.5 mM Gdter, 2 mM EDTA, at 288 K, and an interscan delay of 6 s) to proceed with the spectral assignment. Figure S14 shows the 1D ^{31}P NMR spectra of the E1 extract for a representative liver extract sample. Yet, phosphometabolite concentrations can vary depending on the tissue and the sample. Figure S15 shows a comparison of 1D ^{31}P NMR spectra of all of the tissues that have been studied. Also, some metabolites only appear in the ^{31}P NMR spectrum of a specific tissue or under particular conditions (e.g., hepatocellular carcinoma). Consequently, we first compared 260 spectra from 12 different tissues, identifying a set of up to 94 unambiguous peaks (84 from E1 and 10 from E2 including references, Figure 3), with 29 of them showing an S/N < 5 in a 1D ^{31}P spectrum obtained from 100 mg liver tissue (Figure 3, red numbers).

For peak assignment, we used a combination of chemical shift comparisons and spiking experiments using standard compounds in a concentrated liver sample extract (300 mg). Our initial strategy relied on ^{1}H,^{31}P-HSQMBC-TOCSY experiments, which propagate signals through the coupled protons in each molecule.[29] This approach effectively utilizes the broad chemical shift dispersion of ^{31}P, allowing for the confident assignment of 20 metabolites (Figure S16). However, ^{1}H,^{31}P-HSQMBC-TOCSY is inherently limited by relaxation effects and the complexity of the proton multiplicity patterns. Thus, to expand the list of assigned metabolites, we required the use of the ^{1}H,^{1}H-TOCSY spectra to the spiked spectral data set to assign 11 additional metabolites (Figure S16).

Some metabolites required alternative strategies for assignment. For example, while no reference standard was available

https://doi.org/10.1021/jacsau.5c00234
JACS Au 2025, 5, 2285−2293

for GPE, a combination of G3P and PEA was spiked to generate a pseudo-spin system that closely resembles the one of GPE. Chemical shift analysis of the resulting $^{1}H,^{31}P$-HSQMBC-TOCSY spectrum showed good agreement in the spin system but with an (expected) shift in the proton dimension (Figure S16.R). Other specific metabolites required other tissues with a higher natural abundance to confirm the assignment. This was the case of PCr, whose assignment could be secured only in muscle tissue. Finally, for MPHO, its small size and chemical simplicity (containing a single methyl group) required the independent acquisition of a coupled and a decoupled $^{1}H,^{31}P$-HSQMBC-TOCSY spectra to properly assign the metabolite (Figure S16.AF).

Some ambiguities remain, especially when dealing with metabolites that are chemically similar. For instance, AMP and GMP (or CMP and UMP) were successfully identified using $^{1}H,^{31}P$-HSQMBC-TOCSY, indicating that they are both present in the sample, but they overlap in the 1D ^{31}P spectrum, precluding their individual quantification. Similarly, NDPs and NTPs also present signal overlap in the 1D ^{31}P spectrum, complicating differentiation. $^{1}H,^{31}P$-HSQMBC-TOCSY spectra demonstrated a higher prevalence of adenine and guanine bases as compared to cytosine, thymidine, or uracil. Signal overlaps are also observed for chemically unrelated metabolites, such as 2,3-BPG, F6P, and PEA at 6.74 ppm, particularly when blood contamination is present in the tissue sample (Table S10).

In summary, we could assign 52 of the 82 peaks, corresponding to 37 metabolites in the E1 extract (Tables S10 and S11). From the 32 unknown peaks, an 81.2% (26 peaks) correspond to peaks with an S/N lower than 5 in a standard tissue sample (i.e., 100 mg of liver). The E1 metabolites predominantly represent key intermediates of central carbon metabolism, including glycolysis (G6P, FBP, G3P and 3PG) and the pentose phosphate pathway (S7P and 6PG), which is pivotal for nucleotide synthesis and producing NADPH. On the other hand, multiple nucleotides and nucleotide monophosphate derivatives were identified, including AMP, GMP, UMP, and CMP but they cannot be easily discriminated in the 1D ^{31}P spectrum due to partial signal overlap between the nucleotides (vide supra). Furthermore, it is important to emphasize that these metabolites may undergo chemical hydrolysis during the sample preparation[19] and only the quantification of the total amount of phosphonucleotides becomes meaningful. UDP-sugars, such as UDPG, UDPGal, and UDPNAcGlu, report on glycoconjugate biosynthesis, which is fundamental for glycoprotein and glycolipid formation. The detection of CoA and $FADH_2$ in concentrated sample extracts (i.e., 300 mg) highlights the contribution of mitochondrial oxidative metabolism, particularly in fatty acid β-oxidation and electron transport chain activity. The detection of PCHO, CDPCh, and GPC provides information on phospholipid metabolism, including membrane remodeling and choline-dependent signaling pathways.

The E2 extract produced 9 peaks, and we could assign 7 of them to hydrophobic phosphometabolites that predominantly represent phospholipid components and membrane-associated compounds. PC and PE are structural membrane phospholipids, while PI is a precursor for inositol phosphate signaling pathways, regulating cell growth, metabolism, and apoptosis. SM can be considered as a biomarker of sphingolipid metabolism, with an increasingly recognized role in cell differentiation, membrane microdomain organization, and apoptosis regulation. The presence of lysophospholipids, such as LPC and LPE, suggests active lipid remodeling through phospholipase-mediated hydrolysis, which is crucial in cell membrane dynamics and inflammatory responses. Finally, CL is specific for the mitochondria.

CONCLUSIONS

We here developed new SOPs for both hydrophobic and hydrophilic extracts from tissue using ^{31}P NMR spectroscopy. The SOPs include solvent selection, buffer pH, temperature, osmolality, the use of PREs, reference compounds, and the concentration of chelators, among others, as summarized in Table 1. Our comprehensive optimization of SOPs has markedly improved spectral resolution, signal intensity, dispersion, and the accuracy of metabolite quantification in tissue samples, as reflected by the comparative analysis with other existing methods that were not specifically optimized for this type of samples.

Table 1. SOPs Proposed for Quantitative ^{31}P NMR Analysis for the Hydrophilic and Lipophilic Phosphometabolites

parameter	hydrophilic ^{31}P NMR analysis	lipophilic ^{31}P NMR analysis
solvent	D_2O	d_6-DMSO
buffer and pH	50 mM glycine pD = 9.5	
PRE-agent	Gdter 0.5 mM	
chelator	EDTA 2 mM	
temperature	288 K	310 K
interscan d_1	6 s	5 s

For the E1 extracts, our methodological advancements have established 50 mM glycine buffer at pD 9.5, in D_2O, as the optimal buffer due to its low conductivity and minimal broadening effects, thereby enhancing metabolite stability and spectral quality. Remarkably, the osmolarity invariability among samples results in negligible chemical shift variations for the different extracts, minimizing the effort required for the peak assignment. The inclusion of EDTA as a chelator to neutralize detrimental cation interactions further stabilizes phosphometabolites, ensuring accurate ^{31}P NMR signal quantification. For the E2 extracts, our optimized SOPs emphasize the use of DMSO-d_6 as the solvent, eliminating the need for PREs, which is a critical refinement for preserving the integrity and stability of the lipophilic phosphometabolites.[30] Conducting the analysis at 310 K and setting an interscan delay d_1 of 5 s ensures a balance between T_1 and T_2 relaxation times, leading to enhanced signal quality and reliability in metabolite quantification. These enhancements in methodological approach have enabled detection of up to 94 peaks to identify 44 phosphometabolites. (Figure 2A, Tables S9 and S10). Of the remaining unassigned peaks, 81.8% correspond to very weak peaks that may require the use of higher fields and/or specialized probes for its full characterization.

The study has some limitations: the biphasic extraction of the liver extracts and the required intermediate steps may compromise the absolute quantification and reproducibility of the results. Yet, the repeatability of the assay is very high, indicating that the quantifications are biologically meaningful. In addition, and despite the precautions included in the SOPs, some phosphometabolites (i.e., ATP, NADPH, etc.) shall undergo chemical and/or biological hydrolysis, so the

https://doi.org/10.1021/jacsau.5c00234
JACS Au 2025, 5, 2285−2293

quantifications for the different species of these phosphometabolites must be interpreted cautiously. That said, we believe that our findings represent a significant contribution to the field of metabolomics, setting a new benchmark for excellence in phosphoromic studies.

■ ASSOCIATED CONTENT

Supporting Information

The Supporting Information is available free of charge at https://pubs.acs.org/doi/10.1021/jacsau.5c00234.

NMR spectra for all the assigned metabolites; spectra of different tissues; and data for the different experimental conditions tested (PDF)

■ AUTHOR INFORMATION

Corresponding Authors

Ganeko Bernardo-Seisdedos − *Department of Medicine, Faculty of Health Sciences, University of Deusto, 48007 Bilbao, Spain; ATLAS Molecular Pharma S. L., Parque Tecnológico de Bizkaia, 48160 Derio, Spain*; Email: ganeko.bernardo@deusto.es

Oscar Millet − *Precision Medicine and Metabolism Laboratory, CIC bioGUNE, Basque Research and Technology Alliance, Parque Tecnológico de Bizkaia, 48160 Derio, Spain; CIBERehd, Instituto de Salud Carlos III, 28222 Majadahonda, Spain; ATLAS Molecular Pharma S. L., Parque Tecnológico de Bizkaia, 48160 Derio, Spain*; orcid.org/0000-0001-8748-4105; Email: omillet@cicbiogune.es

Authors

Sara Martin-Ramos − *Precision Medicine and Metabolism Laboratory, CIC bioGUNE, Basque Research and Technology Alliance, Parque Tecnológico de Bizkaia, 48160 Derio, Spain*

Jon Bilbao − *Precision Medicine and Metabolism Laboratory, CIC bioGUNE, Basque Research and Technology Alliance, Parque Tecnológico de Bizkaia, 48160 Derio, Spain*

Tammo Diercks − *NMR Platform, CIC bioGUNE, Basque Research and Technology Alliance, Parque Tecnológico de Bizkaia, 48160 Derio, Spain*; orcid.org/0000-0002-5200-0905

José M. Mato − *Precision Medicine and Metabolism Laboratory, CIC bioGUNE, Basque Research and Technology Alliance, Parque Tecnológico de Bizkaia, 48160 Derio, Spain; CIBERehd, Instituto de Salud Carlos III, 28222 Majadahonda, Spain*

Complete contact information is available at: https://pubs.acs.org/10.1021/jacsau.5c00234

Author Contributions

All authors have given approval to the final version of the manuscript. CRediT: **Sara Martin-Ramos** data curation, formal analysis; **Jon Bilbao** data curation, formal analysis, methodology; **Tammo Diercks** investigation, supervision; **Jose M. Mato** funding acquisition, investigation; **Ganeko Bernardo-Seisdedos** conceptualization, formal analysis, supervision, writing - original draft, writing - review & editing; **Oscar Millet** conceptualization, funding acquisition, writing - original draft, writing - review & editing.

Notes

The authors declare no competing financial interest.

■ ACKNOWLEDGMENTS

Support was provided by the Department of Economic Development and Infrastructures of the Government of the Autonomous Community of the Basque Country (Elkartek bg2021, bg2023). We acknowledge the NMR resources and the technical support provided by the LRE of the Spanish ICTS Red de Laboratorios de RMN de biomoléculas (R-LRB). O.M. and J.M.M. acknowledge CIBERehd and the Agencia Estatal de Investigación (Spain) for grants, RTI2018-101269−B-I00, PID2021-124171OB-I00, and CEX2021-001136-S and NIH for grant NIH 1R01DK119437-01A1.

■ REFERENCES

(1) Bruzzone, C.; Conde, R.; Embade, N.; Mato, J. M.; Millet, O. Metabolomics as a Powerful Tool for Diagnostic, Pronostic and Drug Intervention Analysis in COVID-19. *Front. Mol. Biosci.* **2023**, *10*, No. 1111482.

(2) Ghini, V.; Meoni, G.; Vignoli, A.; Di Cesare, F.; Tenori, L.; Turano, P.; Luchinat, C. Fingerprinting and Profiling in Metabolomics of Biosamples. *Prog. Nucl. Magn. Reson. Spectrosc.* **2023**, *138-139*, 105−135.

(3) Giraudeau, P. Quantitative NMR Spectroscopy of Complex Mixtures. *Chem. Commun.* **2023**, *59* (44), 6627−6642.

(4) Nicholson, J. K.; Jia, W.; Lasky-Su, J. A.; Barbas, C. Metabolic Modeling in Health and Disease. *J. Proteome Res.* **2022**, *21*, No. 559.

(5) Schröter, J.; Popkova, Y.; Süß, R.; Schiller, J. Combined Use of MALDI-TOF Mass Spectrometry and ^{31}P NMR Spectroscopy for Analysis of Phospholipids. *Methods Mol. Biol.* **2017**, *1609*, 107−122.

(6) DeSilva, M. A.; Shanaiah, N.; Gowda, G. A. N.; Rosa-Pérez, K.; Hanson, B. A.; Raftery, D. Application of ^{31}P NMR Spectroscopy and Chemical Derivatization Formetabolite Profiling of Lipophilic Compounds in Human Serum. *Magn. Reson. Chem.* **2009**, *47* (S1), S74−S80.

(7) Kühl, O. *Phosphorus-31 NMR Spectroscopy: A Concise Introduction for the Synthetic Organic and Organometallic Chemist*; Springer, 2009.

(8) Hull, W. E.; Lutz, N. W.; Franks, S. E.; Frank, M. H.; Pomer, S. Investigation of Multidrug Resistance in Cultured Human Renal Cell Carcinoma Cells by ^{31}P-NMR Spectroscopy and Treatment Survival Assays. *Magn. Reson. Mater. Phys., Biol. Med.* **2005**, *18* (3), 144−161.

(9) Fernando, H.; Kondraganti, S.; Bhopale, K. K.; Volk, D. E.; Neerathilingam, M.; Kaphalia, B. S.; Luxon, B. A.; Boor, P. J.; Ansari, G. A. S. ^{1}H and ^{31}P NMR Lipidome of Ethanol-Induced Fatty Liver. *Alcohol.: Clin. Exp. Res.* **2010**, *34* (11), 1937−1947.

(10) Tolman, C. J.; Kanodia, S.; Roberts, M. F.; Daniels, L. ^{31}P-NMR Spectra of Methanogens: 2,3-Cyclopyrophosphoglycerate Is Detectable Only in Methanobacteria Strains. *Biochim. Biophys. Acta, Mol. Cell Res.* **1986**, *886* (3), 345−352.

(11) Bhinderwala, F.; Lonergan, S.; Woods, J.; Zhou, C.; Fey, P. D.; Powers, R. Expanding the Coverage of the Metabolome with Nitrogen-Based NMR. *Anal. Chem.* **2018**, *90* (7), 4521−4528.

(12) Lutz, N. W.; Cozzone, P. J. Principles of Multiparametric Optimization for Phospholipidomics by ^{31}P NMR Spectroscopy. *Biophys. Rev.* **2013**, *5*, 295−304.

(13) Bhinderwala, F.; Evans, P.; Jones, K.; Laws, B. R.; Smith, T.; Morton, M. D.; Powers, R. Phosphorus NMR and Its Application to Metabolomics. *Anal. Chem.* **2020**, *92*, 9536−9545.

(14) Schoeny, H.; Rampler, E.; Chu, D. B.; Schoeberl, A.; Galvez, L.; Blaukopf, M.; Kosma, P.; Koellensperger, G. Achieving Absolute Molar Lipid Concentrations: A Phospholipidomics Cross-Validation Study. *Anal. Chem.* **2022**, *94* (3), 1618−1625.

(15) Furse, S.; Williams, H. E. L.; Watkins, A. J.; Virtue, S.; Vidal-Puig, A.; Amarsi, R.; Charalambous, M.; Koulman, A. A Pipeline for

Making ^{31}P NMR Accessible for Small- and Large-Scale Lipidomics Studies. *Anal. Bioanal. Chem.* **2021**, *413* (19), 4763−4773.
(16) Mulder, F. A. A.; Tenori, L.; Luchinat, C. Fast and Quantitative NMR Metabolite Analysis Afforded by a Paramagnetic Co-Solute. *Angew. Chem., Int. Ed.* **2019**, *58* (43), 15283−15286.
(17) Cox, N.; Millard, P.; Charlier, C.; Lippens, G. Improved NMR Detection of Phospho-Metabolites in a Complex Mixture. *Anal. Chem.* **2021**, *93* (11), 4818−4824.
(18) Bernardo-Seisdedos, G.; Bilbao, J.; Fernández-Ramos, D.; Lopitz-Otsoa, F.; de Juan, V. G.; Bizkarguenaga, M.; Mateos, B.; Fondevila, M. F.; Abril-Fornaguera, J.; Diercks, T.; Lu, S. C.; Nogueiras, R.; Mato, J. M.; Millet, O. Metabolic Landscape of the Mouse Liver by Quantitative ^{31}P Nuclear Magnetic Resonance Analysis of the Phosphorome. *Hepatology* **2021**, *74* (1), 148−163.
(19) Bhinderwala, F.; Lei, S.; Woods, J.; Rose, J.; Marshall, D. D.; Riekeberg, E.; Leite, A. D. L.; Morton, M.; Dodds, E. D.; Franco, R.; Powers, R. Metabolomics Analyses from Tissues in Parkinson's Disease. *Methods Mol. Biol.* **2019**, *1996*, 217−257.
(20) Moision, R. M.; Armentrout, P. B. An Experimental and Theoretical Dissection of Potassium Cation/Glycine Interactions. *Phys. Chem. Chem. Phys.* **2004**, *6* (10), 2588−2599.
(21) Moision, R. M.; Armentrout, P. B. Experimental and Theoretical Dissection of Sodium Cation/Glycine Interactions. *J. Phys. Chem. A* **2002**, *106* (43), 10350−10362.
(22) Fedotova, M. V.; Kruchinin, S. E. Ion-Binding of Glycine Zwitterion with Inorganic Ions in Biologically Relevant Aqueous Electrolyte Solutions. *Biophys. Chem.* **2014**, *190*−*191*, 25−31.
(23) Lutz, N. W.; Bernard, M. Methodological Developments for Metabolic NMR Spectroscopy from Cultured Cells to Tissue Extracts: Achievements, Progress and Pitfalls. *Molecules* **2022**, *27*, No. 4214.
(24) Bosco, M.; Culeddu, N.; Toffanin, R.; Pollesello, P. Organic Solvent Systems for ^{31}P Nuclear Magnetic Resonance Analysis of Lecithin Phospholipids: Applications to Two-Dimensional Gradient-Enhanced 1H-Detected Heteronuclear Multiple Quantum Coherence Experiments. *Anal. Biochem.* **1997**, *245* (1), 38−47.
(25) Vasavada, K. V.; Ray, B. D.; Rao, B. D. N. ^{31}P NMR Lineshapes of β-P (ATP) in the Presence of Mg^{2+} and Ca^{2+}: Estimate of Exchange Rates. *J. Inorg. Biochem.* **1984**, *21* (4), 323−335.
(26) Hafer, E.; Holzgrabe, U.; Kraus, K.; Adams, K.; Hook, J. M.; Diehl, B. Qualitative and Quantitative ^{1}H NMR Spectroscopy for Determination of Divalent Metal Cation Concentration in Model Salt Solutions, Food Supplements, and Pharmaceutical Products by Using EDTA as Chelating Agent. *Magn. Reson. Chem.* **2020**, *58* (7), 653−665.
(27) Shenderovich, I. G. Experimentally Established Benchmark Calculations of 31 P NMR Quantities. *Chem.: Methods* **2021**, *1* (1), 61−70.
(28) Lutz, N. W.; Yahi, N.; Fantini, J.; Cozzone, P. J. Analysis of Individual Purine and Pyrimidine Nucleoside Di- and Triphosphates and Other Cellular Metabolites in PCA Extracts by Using Multi-nuclear High Resolution NMR Spectroscopy. *Magn. Reson. Med.* **1996**, *36* (5), 788−795.
(29) Gowda, G. A. N.; Pascua, V.; Killion, C. E.; Paranji, R. K.; Raftery, D. Labile Metabolite Profiling in Human Blood Using Phosphorus NMR Spectroscopy. *Anal. Chem.* **2023**, *95* (40), 15033−15041.
(30) Furse, S.; Egmond, M. R.; Killian, J. A. Isolation of Lipids from Biological Samples. *Mol. Membr. Biol.* **2015**, 55−64.

https://doi.org/10.1021/jacsau.5c00234
JACS Au 2025, 5, 2285−2293